J Therm Anal Calorim (2011) 105:793–803
DOI 10.1007/s10973-010-1242-6

Influence of gas media on the thermal decomposition of second valence iron sulphates

V. Petkova · Y. Pelovski · D. Paneva · I. Mitov

ESTAC2010 Conference Special Issue

Abstract $FeSO_4 \cdot H_2O$ and $FeSO_4$ represent the second valence of iron sulphates. Number of studies has been done to understand formation of intermediate sulphates like $FeOHSO_4$ and $Fe_2O(SO_4)_2$, representing the oxidation of Fe^{2+} to Fe^{3+}. At selected temperatures, both the thermodynamical equilibrium in the Fe–S–O system and the formation of the crystal structures in the solid phase are controlled by the partial pressure of water vapour and oxygen in the gas phase. The effects of the temperature and the partial pressure of gas components on the solid-phase content are demonstrated by phase diagrams. The study puts the accent on the influence of oxygen content in gas environment on processes of thermal decomposition of $FeSO_4 \cdot H_2O$ and $FeSO_4$. At three quantities of oxygen content—0% (100% Ar), 21% (dry air) and 100% (pure O_2) the processes of oxidation and formatting metastable iron sulphates were examined by several experimental techniques. The thermal decomposition of samples was investigated by TG–DTG–DTA method in the temperature range 293–1400 K. Partial pressure of water vapour was determined by the quantity of water released from dehydration process of $FeSO_4 \cdot H_2O$. Infrared spectroscopy, Mössbauer spectroscopy and X-Ray powder diffraction method were used for identification of the new formed solid structures and for characterization of the content of the iron sulphates with different valencies of iron. The experimental data and their analyses give the possibility to determine the different stages of decomposition, related to the formation of intermediates. Depending on gas environment, the basic relationships for reaction kinetics is drawn. It is demonstrated on that correlation exists between the kinetic's parameters and the content of oxygen in the gas phase.

Keywords Iron sulphates · Thermal decomposition · X-Ray · IR spectroscopy · Mössbauer spectroscopy

V. Petkova (✉)
Institute of Mineralogy and Crystallography,
Bulgarian Academy of Sciences,
Acad. G. Bonchev Str., Bl. 107, 1113 Sofia, Bulgaria
e-mail: vilmapetkova@gmail.com

Y. Pelovski
University of Chemical Technology and Metallurgy,
8 Kl. Ohridski Str, 1756 Sofia, Bulgaria

D. Paneva · I. Mitov
Institute of Catalysis, Bulgarian Academy of Sciences,
Acad. G. Bonchev Str., Bl. 10, 1113 Sofia, Bulgaria

Introduction

Iron belongs to the group of transition metals due to the possible participation of electrons from the inner electronic layers in chemical interactions. Ferrous iron (Fe^{2+}) may be oxidized to ferric iron (Fe^{3+}) by the loss of an electron, which depends on the experimental conditions. Ferrous sulphate ($FeSO_4 \cdot xH_2O$, $x \leq 7$, divalent iron) and ferric sulphate ($Fe_2(SO_4)_3 \cdot xH_2O$, $x \leq 9$, trivalent iron) are typical iron salts. They are widely used in inorganic technology practice as precursors for the synthesis and investigation of phase transformations of iron oxides [1, 2], for the production of pigments [3–9] and in pyrite concentrate oxidative roasting process [10–15]. The scientific interest in such minerals and their thermal stability is determined by the possible identification of these minerals and related dehydrated materials from the surface of Mars [16, 17]. In all application of iron sulphate it is necessary to take account the possibility of oxidation of Fe^{2+} to Fe^{3+}. This fact is particularly important in the processes of thermal

decomposition of $FeSO_4 \cdot xH_2O$, where the possible thermal effects of formation and decomposition of $FeOHSO_4$ and $Fe_2O(SO_4)_2$ depends on the temperature and the presence of oxygen in the gas phase [18–22].

Our previous publications show that the formation of $Fe_2O(SO_4)_2$ is more difficult than $FeOHSO_4$, and this process depends both on the temperature and the partial pressures of gaseous components—oxygen, water vapour and sulphur oxides [18–21]. The published results indicate that the presence of oxidative or inert gas is one of important parameters that influence the process of the thermal decomposition of divalent iron sulphates.

As a continuation of these studies, this study puts the accent on the influence of gas environment (inert and oxidative) on the processes of thermal decomposition both of $FeSO_4 \cdot H_2O$ and $FeSO_4$. In addition, this study aims to determine the conditions of formation and decomposition of metastable iron sulphates. To prevent the partial oxidation of ferrous sulphates to ferric sulphates, the purity of the samples is necessary to achieve.

Experimental

Samples

$FeSO_4$ was produced by a heating of $FeSO_4 \cdot 7H_2O$ at 743 K (heating rate of 10 K min^{-1}) in a medium of 100% Ar. $FeSO_4 \cdot H_2O$ was produced by a preliminary drying of $FeSO_4 \cdot 7H_2O$ at 353 K in a vacuum of 0.6×10^{-5} Pa. The dried product contained 55.93% SO_4^{2-}, 34.57% Fe^{2+} and 9.5% crystal water [18].

Methods

The X-ray powder diffraction (XRD) measurements of the samples were performed on a DRON 3M diffractometer with a horizontal Bragg–Brentano goniometer (radius of 192 mm) using a Fe-filtered Co-Kα radiation (40 kV, 28 mA). A step-scan technique was applied with a step size of 0.02°2θ and 3 s per step in the range 8°–60°2θ.

The diffractometer was externally calibrated with quartz and Si standards. Before the XRD experiments, the samples were ground in agate mortar, and the front-loaded pressed powder specimens were measured at room temperature.

The precise position, intensity and broadening (FWHM) of the peaks in the XRD patterns of the samples were determined by profile fitting using the WinFit V1.2 package [23]. The unit cell parameters were refined by the program PowderCell [24]. For determination of the phases and minerals present in the samples, the database PDF (Powder Diffraction File, ICDD, 2001) [25] was used.

The vibration and deformation deviations of SO_4^{2-} and OH^- of the FTIR spectra (KBr pellets) were recorded on a Bruker Tensor 37 spectrometer. To collect 120 scans for each sample, the resolution of 2 cm^{-1} was used.

The Mössbauer spectra were obtained with an electromechanical spectrometer ("Wissenschaftliche Elektronik" GmbH), working with constant acceleration mode at room temperature. A 57Co/Cr source and an α-Fe standard were used. The experimentally obtained spectra were processed mathematically by least squares method. The parameters of hyperfine interaction such as isomer shift (IS), quadrupole splitting (QS) and effective internal magnetic field (H_{eff}) as well as the line widths (FWHM) and the relative weight of spectral partial components (G) were determined.

The TG–DTG–DTA-analyses were conducted with thermal complex Stanton Redcroft (England). The samples with mass of 10.0 ± 0.2 mg were studied in the temperature range 293–1400 K at heating rate of 10 K min^{-1}. Zirconium crucibles were used with diameter of 4.5 mm.

The experiments were carried out with three types of flowing gas—100% Ar, 100% Air (dried and purified) and 100% O_2 at a rate of 50 mL min^{-1}. Thus at chosen gas environments, the oxygen content varied from 0% (100% Ar) to 100% (O_2) which allow to study the effect of oxygen content on the processes of oxidation and obtaining the metastable iron sulphates. The other experimental conditions were kept the same to ensure correctness and comparability of experimental results.

Results

X-ray phase analysis

The results of X-ray phase and structure analyses are shown in Fig. 1 a and b and Table 1. These spectra correspond to the diffraction lines $FeSO_4 \cdot H_2O$ (PDF 45-1365, d/nm: 0.345, 0.310, 0.253) and $FeSO_4$ (PDF 17-0873, d/nm: 0.263, 0.365, 0.341). The experimental data for the lattice parameters are in good agreement with references. The spectral lines of $FeSO_4$ (Fig. 1b) are with low intensity, probably as a result of the method of obtaining the anhydrous ferrous sulphate. Nevertheless, the main phase is $FeSO_4$ because the diffraction lines of other trivalent iron sulphates ($FeOHSO_4$ or $Fe_2O(SO_4)_2$) are not registered.

Infrared spectroscopy

The IR spectroscopies of samples are shown in Fig. 2 a and b. The symmetric bending mode (ν_2) of SO_4^{2-} is enhanced with medium peak intensity for $FeSO_4$ at 480 cm^{-1} (Fig. 2b) and low peak intensity for $FeSO_4 \cdot H_2O$ [26]. The asymmetric bending mode (ν_4) of SO_4^{2-} is presented as

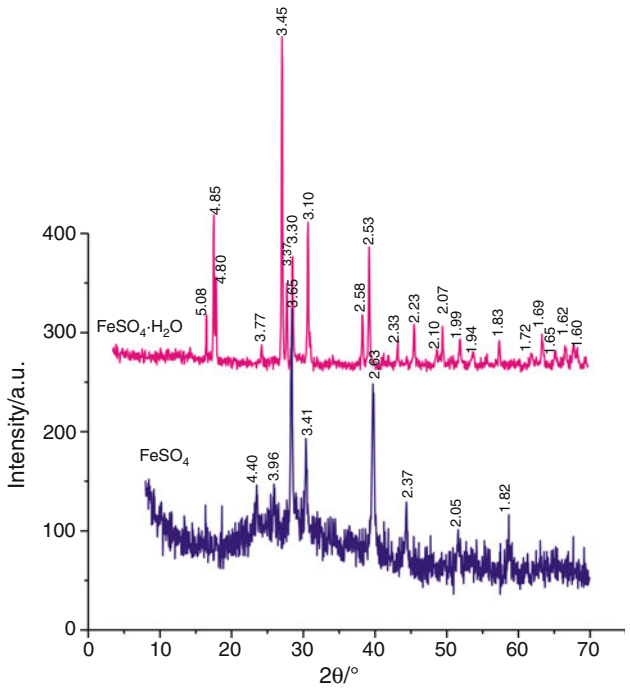

Fig. 1 XRD patterns of: **a** $FeSO_4{\cdot}H_2O$; **b** $FeSO_4$

Table 1 Mean crystallite size (D), micro-strain (E), and unit cell parameters (a and c), of $FeSO_4{\cdot}H_2O$ and $FeSO_4$

Sample	$FeSO_4{\cdot}H_2O$				$FeSO_4$			
	D/nm	$E \times 10^{-4}$	a/nm	c/nm	D/nm	$E \times 10^{-4}$	a/nm	c/nm
1[a]	–	–	7.075	7.600	–	–	5.252	6.590
2[b]	112.63	8.13	7.083	7.601	42.22	8.52	5.250	6.593

[a] ICSD collection code 27098 for $FeSO_4{\cdot}H_2O$ and ICSD collection code 23507 for $FeSO_4$

[b] The samples of $FeSO_4{\cdot}H_2O$ and $FeSO_4$, are obtained in conditions, described in Sect. "Samples"

triplet at 604, 624 and 667 cm^{-1} ($FeSO_4{\cdot}H_2O$) and a doublet at 601 and 684 cm^{-1} ($FeSO_4$). The asymmetrical stretching mode (ν_3) of SO_4^{2-} is split into two peaks, due to lower symmetry: 1090 and 1159 cm^{-1} for $FeSO_4{\cdot}H_2O$ (Fig. 2a); 1066 and 1170 cm^{-1} for $FeSO_4$ (Fig. 2b). The symmetrical stretching mode (ν_1) of SO_4^{2-} is registered at 997 cm^{-1} for $FeSO_4$, and slight shift to 1018 cm^{-1} for $FeSO_4{\cdot}H_2O$.

The distribution of absorption lines, related to the vibration of water molecules, identify the peaks of structural (OH^-) and crystal water. The ν_3 bands of OH^- are located at 3409 cm^{-1} ($FeSO_4{\cdot}H_2O$) and 3464 cm^{-1} ($FeSO_4$), which indicates the existence of crystal water in the structure of sulphates. The ν_2 bands of crystal water are registered at 1637 cm^{-1} (Fig. 2). The broad band of OH^- in the range 3000–3260 cm^{-1} of the spectrum of $FeSO_4{\cdot}H_2O$ (Fig. 2a) is associated with strong hydrogen bonds.

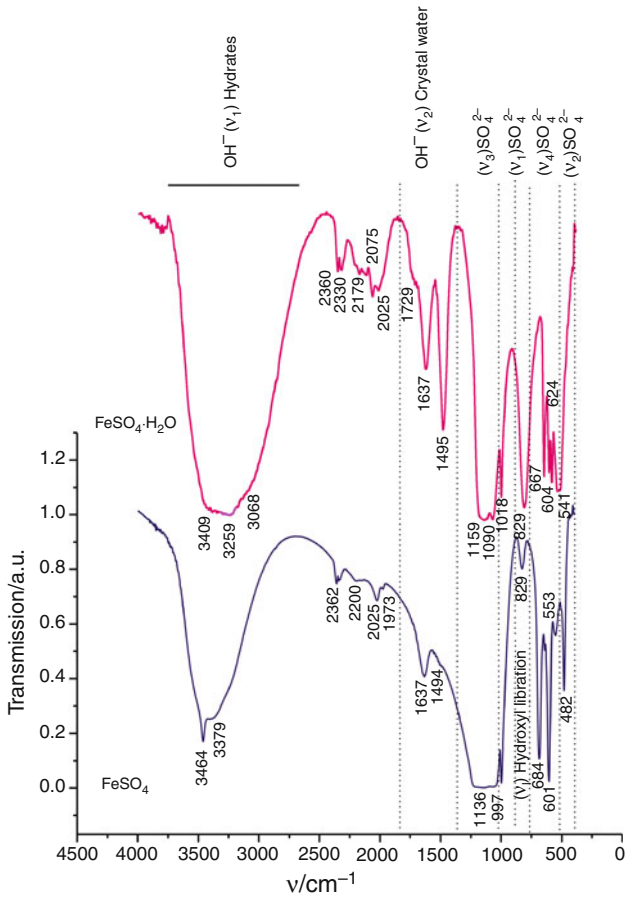

Fig. 2 IR spectrums of: **a** $FeSO_4{\cdot}H_2O$; **b** $FeSO_4$

The ν_2 bands of the hydroxyl group are registered at 1495 cm^{-1} ($FeSO_4{\cdot}H_2O$) and with low intensity at 1494 cm^{-1} ($FeSO_4$) (Fig. 2). The ν_4 bands of OH^- are located at 541 and 829 cm^{-1} ($FeSO_4{\cdot}H_2O$) and 550 and 829 cm^{-1} ($FeSO_4$). The low intensity of IR bands (ν_2—1494 cm^{-1}, ν_4—829 and 550 cm^{-1}) of anhydrous ferrous sulphate shows the presence of very small amount of structural water in the sample. This effect is due to the absorbing water vapour from the air, which confirms the strong hygroscopicity of iron sulphates, found in our previous publications [18, 19].

Mössbauer spectroscopy

The results of Mössbauer spectroscopy of $FeSO_4{\cdot}H_2O$ and $FeSO_4$ are shown in Fig. 3 a and b. The determined parameters of ultrafine interaction are shown in Table 2. The Mössbauer spectra include doublets of Fe^{2+} in high-spin state. The determined Mössbauer hyperfine parameters (isomer shift and quadrupole splitting) indentify that the $FeSO_4{\cdot}H_2O$ and $FeSO_4$ are the main iron-containing phases in the samples. The other physical experimental methods

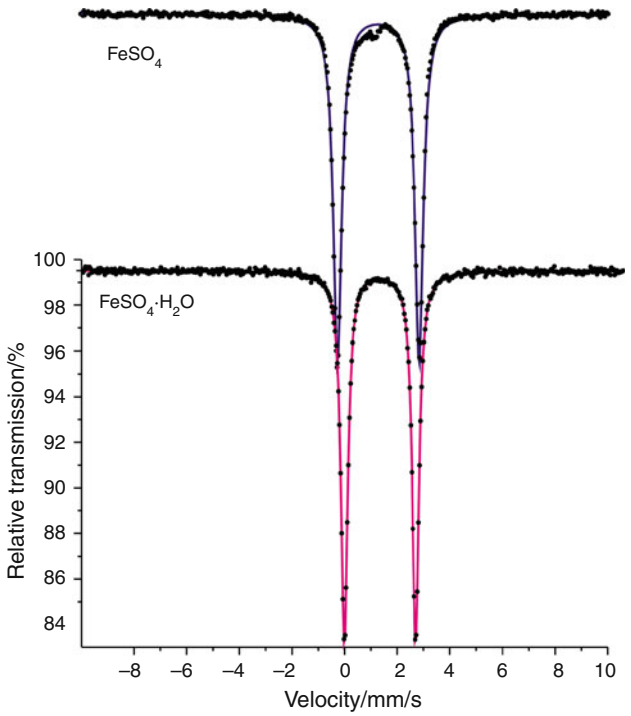

Fig. 3 Mössbauer spectrums of: **a** $FeSO_4{\cdot}H_2O$; **b** $FeSO_4$

characterize these products as monophase. These results for the purity of the samples are essential for further analysis of their thermal behaviour.

Thermal analysis

The results of thermal experiments of $FeSO_4{\cdot}H_2O$ and $FeSO_4$ in various gas environments are shown in Fig. 4 and Table 3. Based on the registered and calculated thermal TG, DTG and DTA curves the reactions of dehydration and decomposition of the samples are analyzed.

$FeSO_4{\cdot}H_2O$, 100% Ar gas environment

The thermal decomposition of $FeSO_4{\cdot}H_2O$ in 100% Ar gas environment is characterized with three stages of mass losses, observed by three endothermic peaks in the DTA curve (Fig. 4a and Table 3). It is supposed that in the absence of oxidative agent in the gas environment, the dehydration of the last molecule of crystal water to anhydrous ferrous sulphate is realized with mass losses close to the theoretical ($\Delta G_{\text{theor}} = 10.59\%$, dehydration reaction). The mass losses for process of dehydration are lower than theoretical ones (8.50%), which can be explained that monohydrate contains non-stoichiometric amount of crystal water.

Table 2 Mössbauer parameters of studied samples

Sample	Components	IS/ mm/s	QS/ mm/s	H_{eff}/ T	FWHM/ mm/s	*G*/ %
$FeSO_4{\cdot}H_2O$	$FeSO_4{\cdot}H_2O$	1.25	2.71	–	0.29	100
$FeSO_4$	$FeSO_4$	1.28	3.10	–	0.38	100

The TG and DTG dependencies in next high temperature range (800–870 K) show two overlapping thermal reactions, which were also observed by other authors [27, 28]. It is suggested that the obtained $FeSO_4$ is transformed into an intermediate trivalent sulphate—$Fe_2O(SO_4)_2$ or $Fe_2(SO_4)_3$. Masset et al. [27] proposed that $Fe_2(SO_4)_3$ is obtained at the thermal treatment of $FeSO_4{\cdot}H_2O$ in an inert gas environment. They prove the formation of $Fe_2(SO_4)_3$ with an analysis of evolving gases, where both the sulphur oxides and oxygen were identified ($SO_3 \rightarrow SO_2 + 1/2O_2$)—reaction A.

$$6FeSO_4 = Fe_2(SO_4)_3 + 2\alpha\text{-}Fe_2O_3 + 3SO_2 \qquad (A[27])$$

The composition of the gas phase at the decomposition to $Fe_2O(SO_4)_2$ is the same—reaction B.

$$4FeSO_4 = Fe_2O(SO_4)_2 + \alpha\text{-}Fe_2O_3 + 2SO_2 \qquad (B)$$

The phase diagram of Fe–S–O system at 500 K (Fig. 5) was presented in our previous publication [18]. The maintaining a high partial pressure of sulphur oxides is a necessary condition for the formation of $Fe_2(SO_4)_3$. When the inert gas flowing is used, the obtained sulphur oxides are continuously removed from the reaction space, without ensuring required level of partial pressure to obtain the $Fe_2(SO_4)_3$.

Conversely, for the formation of $Fe_2O(SO_4)_2$ a high content of sulphur oxides is not necessary [18, 19]. Thus in our experimental conditions it is suggested that the formation of $Fe_2O(SO_4)_2$ is more probable than the formation of $Fe_2(SO_4)_3$. There are good match between the theoretical (10.90%) and experimental (10.00%) mass losses.

The obtained $Fe_2O(SO_4)_2$ and remaining $FeSO_4$ are decomposed in the temperature range 870–1010 K (third stage of decomposition) to hematite and sulphur oxides [18] ($\Delta G_{\text{theor}} = 27.20\%$). The suggested reactions at lower temperatures are confirmed with the registered higher mass losses (31.10%), due to the iron oxysulphate formation. The suggestion of formation of $Fe_2O(SO_4)_2$ instead of $Fe_2(SO_4)_3$ is substantiated with low value of mass losses, (<35%—decomposition of ferric sulphate). Based on these results offered, the following set of reactions is proposed to explain the process of thermal decomposition of $FeSO_4{\cdot}H_2O$ (100% Ar gas environment) in the temperature range 290–1400 K:

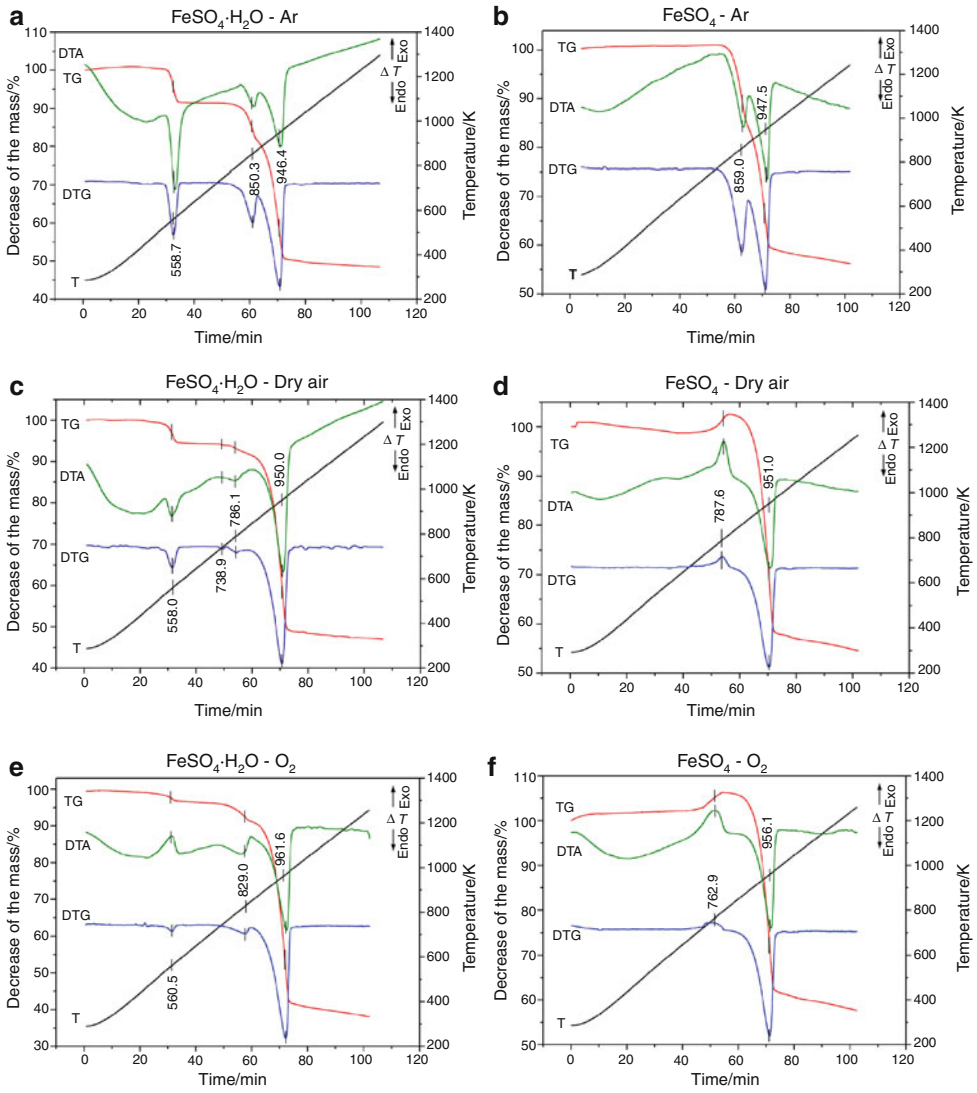

Fig. 4 TG–DTG–DTA curves of: **a** $FeSO_4 \cdot H_2O$ in 100% Ar; **b** $FeSO_4$ in 100% Ar; **c** $FeSO_4 \cdot H_2O$ in 100% Air; **d** $FeSO_4$ in 100% Air; **e** $FeSO_4 \cdot H_2O$ in 100% O_2; **f** $FeSO_4$ in 100% O_2

I. 500–610 K—dehydration

$$FeSO_4 \cdot H_2O = FeSO_4 + H_2O \quad (1)$$

II. 800–870 K—partial decomposition

$$4FeSO_4 = Fe_2O(SO_4)_2 + \alpha\text{-}Fe_2O_3 + 2SO_2 \quad (2B)$$

III. 870–1010 K—decomposition

$$Fe_2O(SO_4)_2 = \alpha\text{-}Fe_2O_3 + 2SO_2 + O_2 \quad (3)$$

$$2FeSO_4 = \alpha\text{-}Fe_2O_3 + 2SO_2 + 1/2O_2 \quad (4)$$

$FeSO_4$, 100% Ar gas environment

The thermal decomposition of $FeSO_4$ in 100% Ar gas environment is characterized with two overlapping thermal reactions in the temperature range 780–920 K (Fig. 4b and Table 3). The first one is probably the partial conversion of $FeSO_4$ to an oxysulphate according reaction (2). The registered mass losses for this stage are 17.00%, which are lower than theoretical ones ($\Delta G_{theor} = 21.08\%$) in this temperature range. The second reaction of decomposition overlaps the first one, thus the mass losses of solid mixture of $FeSO_4$ and $Fe_2O(SO_4)_2$ in the temperature range 850–980 K are 25.10%. The comparison between theoretical (26.35%) and experimental mass losses shows a good match (Fig. 4b and Table 3). Thus, the thermal decomposition of anhydrous ferric sulphate in 100% Ar gas environment is characterized by reactions (2) and (4).

$FeSO_4 \cdot H_2O$, dry air gas environment

The thermal decomposition of $FeSO_4 \cdot H_2O$ in dry air gas environment may be divided into three stages (Fig. 4c and Table 3). The first stage is in the temperature range 520–600 K, where 4.60% mass lossess is realized. Because this temperature range is identical to first stage of decomposition of $FeSO_4 \cdot H_2O$ in inert gas environment, the observed effects are due to the dehydration of the last

Table 3 Temperature ranges and mass losses, determined at thermal decomposition of $FeSO_4$ and $FeSO_4{\cdot}H_2O$ in various gas environments

Stage	$FeSO_4{\cdot}H_2O$				$FeSO_4$			
	T_{infl}/K	T_{start}/K	T_{end}/K	ΔG/%	T_{infl}/K	T_{start}/K	T_{end}/K	ΔG/%
100% Ar								
1	558.7	509.4	602.7	8.5	–	–	–	–
2	850.3	804.9	872.6	10.0	859.0	763.1	855.6	17.0
3	946.4	872.6	1009.4	31.1	947.5	855.6	984.1	25.1
Total				51.5				45.0
100% Air								
1	558.0	522.5	594.9	4.6	–	–	–	–
2	786.1	754.2	847.6	2.5	771.3	732.7	813.7	+3.4
3	950.0	847.6	1016.0	42.7	930.0	813.7	997.2	44.8
Total				53.0				48.0
100% O_2								
1	560.5	481.4	597.4	2.2	–	–	–	–
2	829.0	714.6	850.3	5.0	762.9	663.4	831.6	+4.1
3	965.5	850.3	1019.2	50.1	956.1	831.6	1004.3	45.0
Total				61.5				49.7

T_{infl}—temperature inflection point/K

T_{start}—initial temperature of the stage/K

T_{end}—final phase temperature/K

ΔG—mass losses for the stage/%

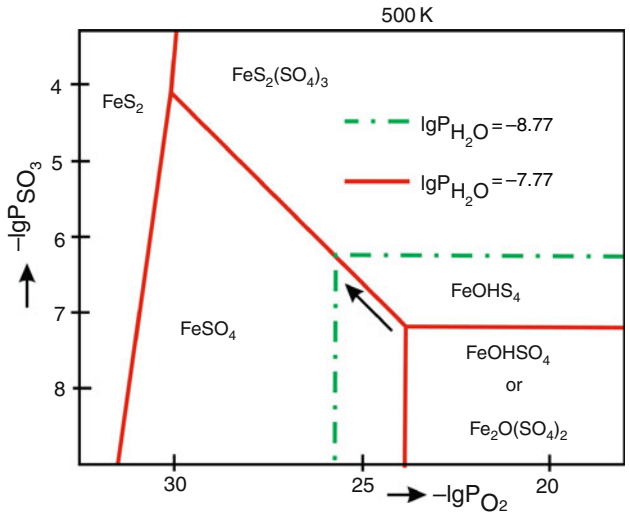

Fig. 5 Phase diagram of Fe–S–O system at 500 K [18]

molecule of crystal water from monohydrate (ΔG_{theor} = 10.59%) with obtaining of $FeSO_4$. The registered mass losses are two times smaller (4.60%) than the theoretically possible. This circumstance may be explained with some retention of a crystal water in the solid phase, caused by formation of metastable trivalent iron sulphate ($FeOHSO_4$) during the reaction of partial oxidation of $FeSO_4{\cdot}H_2O$. The reaction space contains oxygen, which takes part in the reactions of oxidation of Fe^{2+} to Fe^{3+}. The metastable trivalent iron sulphates are obtained by solid-phase synthesis. This oxidative reaction is possible due to the appropriate temperature range and the presence of water vapour (dehydration) and oxygen (dry air flowing). These conditions predetermine that the formation of the hydroxysulphate is more thermodynamically possible than the oxysulphate [18, 19].

The mass losses in second stage of decomposition in the temperature range 740–850 K are approximately 3.00%. It is suggested that the registered endothermic effect of a very low intensity is a result of two reactions with compensation of heat effects—a separation of OH^- from $FeOHSO_4$ (endothermic effect) and oxidation of $FeSO_4$ to $Fe_2O(SO_4)_2$ (exothermic effect). The mass losses show that these reactions are incomplete, so both $FeSO_4$ and $Fe_2O(SO_4)_2$ are present at the end of the temperature range. These sulphates are decomposed to hematite and sulphur oxides [18] in the last stage of the studied process (T_{infl} = 930 K).

The process of thermal decomposition of $FeSO_4{\cdot}H_2O$ (dry air gas environment) in the temperature range 290–1400 K is proposed to explain with the following set of reactions:

I. 520–600 K—dehydration and oxidation

$$FeSO_4 \cdot H_2O = FeSO_4 + H_2O \quad (1)$$

$$2FeSO_4 \cdot H_2O + 1/2O_2 = 2FeOHSO_4 + H_2O \quad (5)$$

II. 740–850 K—dehydration and oxidation

$$2FeOHSO_4 = Fe_2O(SO_4)_2 + H_2O \quad (6)$$

$$2FeSO_4 + 1/2O_2 = Fe_2O(SO_4)_2 \quad (7)$$

III. 850–1020 K—decomposition

$$2FeSO_4 = \alpha\text{-}Fe_2O_3 + 2SO_2 + 1/2O_2 \quad (4)$$

$$Fe_2O(SO_4)_2 = \alpha\text{-}Fe_2O_3 + 2SO_2 + O_2 \quad (3)$$

$FeSO_4$, dry air gas environment

The comparison between the thermograms of $FeSO_4{\cdot}H_2O$ and $FeSO_4$ shows that they are completely different (Fig. 4c, d and Table 3). Moreover the type of used flowing gas strongly influences on the thermal decomposition of $FeSO_4$ (Fig. 4b, d). The process is characterized by two distinct stages. In the first stage an intense exothermic reaction with increased mass of sample is registered. In the second stage an endothermic reaction with loss of mass is observed. In dry air environment without the presence both of water vapour and sulphur oxides in the temperature range 730–820 K the thermodynamical equilibrium is shifted to the area of stability of $Fe_2O(SO_4)_2$ (Fig. 5). The theoretically possible increase of the mass of the samples is 5.30%, but only 3.40% is determined experimentally. This shows that at the chosen experimental conditions—rate of heating of 10 K min^{-1} and

limited oxygen in the gas phase (~21%)—the reaction is incomplete. In the second stage, the obtained solid-phase products are decomposed to a hematite and sulphur oxides. Thus the process of thermal decomposition of $FeSO_4$ in dry air gas environment is in accordance with reactions (7), (4) and (3). The determined mass losses (48.00%) are higher than the theoretically possible for the decomposition of pure $FeSO_4$ ($\Delta G_{theor} = 47.40\%$) and lower than those for the decomposition of $Fe_2O(SO_4)_2$ ($\Delta G_{theor} = 50.03\%$). This may be explained with an incomplete oxidation of $FeSO_4$ to $Fe_2O(SO_4)_2$.

$FeSO_4 \cdot H_2O$, 100% O_2 gas environment

The TG and DTA dependencies of thermal decomposition of $FeSO_4 \cdot H_2O$ in 100% O_2 gas environment (Fig. 4e and Table 3) are different from these for other gas environments. The first losses (2.20%) are registered in the temperature range 480–600 K, where a strong exothermic peak on the DTA ($T_{infl} = 560.5$ K) is noticed. It is interesting to note that in this temperature range the decomposition of the monohydrate at other gas environments is characterized with an endothermic peak (Fig. 4a, c and Table 3). The exothermic reaction may be explained by two overlapping direct oxidations of $FeSO_4 \cdot H_2O$: to $FeOHSO_4$ ($\Delta G_{theor} = 0.59\%$) and to $Fe_2O(SO_4)_2$ ($\Delta G_{theor} = 5.88\%$). The $FeOHSO_4$ is a low temperature modification obtained at certain partial pressure of water vapour [18, 19, 29–31]. The presence of water vapour in gas environment is determined by dehydration of $FeSO_4 \cdot H_2O$. Thus, the conditions for predominantly obtaining of ferric hydroxysulphate in a solid phase (appropriate temperature and presence both of the water vapour and the oxygen) are satisfied. It is supposed that the second reaction is lateral side oxidation (to $Fe_2O(SO_4)_2$), which is possible at high partial pressure of oxygen in the gas phase. This suggestion is confirmed with registered mass losses (2.20%), which are result of an oxidation of $FeSO_4 \cdot H_2O$ to $FeOHSO_4$ and partial obtaining of ferric oxysulphate. This analysis is based on the assumption that the obtained solid phase is a mixture of $FeOHSO_4$ and $Fe_2O(SO_4)_2$ [18]. In the high temperature region, two coupled endothermic reactions with $T_{infl} = 829.0$ and 961.6 K may be found (Fig. 4e, Table 3): dehydration of structural water (OH^-) from ferric hydroxysulphate with obtaining of $Fe_2O(SO_4)_2$ ($\Delta G_{theor} = 5.27\%$) and decomposition of $Fe_2O(SO_4)_2$ to hematite and sulphur oxides ($\Delta G_{theor} = 50.03\%$). These values are almost equal to the experimental results for mass losses—5.00 and 50.10%, respectively. These results are evidence for the proposed mechanisms of decomposition in two temperature regions.

The comparison between temperature ranges of decomposition of $Fe_2O(SO_4)_2$ in the various gas environments shows an shift to higher temperatures of increasing the oxygen content. The presence of oxygen, obtained during oxidation and decomposition of $FeSO_4 \cdot H_2O$, delays the thermal processes, respectively increase the temperatures of the reaction.

These results for thermal decomposition of $FeSO_4 \cdot H_2O$ in environment of pure oxygen in the temperature range 290–1400 K and their analysis may be summarised as following set of reactions:

I. I 480–600 K—dehydration and oxidation

$$2FeSO_4 \cdot H_2O + 1/2O_2 = 2FeOHSO_4 + H_2O \quad (5)$$

$$2FeSO_4 \cdot H_2O + 1/2O_2 = Fe_2O(SO_4)_2 + 2H_2O \quad (8)$$

II. 710–850 K—dehydration

$$2FeOHSO_4 = Fe_2O(SO_4)_2 + H_2O \quad (6)$$

III. 850–1020 K—decomposition

$$Fe_2O(SO_4)_2 = \alpha\text{-}Fe_2O_3 + 2SO_2 + O_2 \quad (3)$$

$FeSO_4$, 100% O_2 gas environment

The thermal decomposition of $FeSO_4$ in 100% O_2 gas environment (Fig. 4f and Table 3) is similar to the thermal decomposition of $FeSO_4$ in dry air gas environment (Fig. 4d and Table 3). The overall process may be divided into two processes—an oxidation and a decomposition. The thermal decomposition of $FeSO_4$ in temperature range 660–830 K at high partial pressure of oxygen without the presence both of water vapour and sulphur oxides leads to formation of $Fe_2O(SO_4)_2$, which is a thermostable solid phase. This is confirmed with mass losses in this temperature range, where the mass of sample is increased with 4.10% ($\Delta G_{theor} = 5.27\%$). The solid-phase synthesis of $Fe_2O(SO_4)_2$ is reaction (4) with higher conversion rate than in dry air gas environments (+3.40%, Table 3). In the temperature range of 830–1000 K, the decomposition of $Fe_2O(SO_4)_2$ occurs. The experimental mass losses of 49.70% are commensurable to the theoretical ones—50.03% (Table 3). Thus, the thermal decomposition of anhydrous $Fe_2O(SO_4)_2$ in 100% O_2 gas environment is described by reactions (3).

Discussion

The comparative studies of thermal decompositions of sulphates of divalent iron in various gas environments allow evaluating the basic principles both of the chemical reaction and the kinetics of studied processes. In our previous publications [18, 19] it was proven that the oxygen and the water vapour strongly affect on the obtaining of the metastable sulphates of trivalent iron. Both the partial

pressure and the ratio between oxygen and water vapour in gas phase control the process of obtaining the monophase products in the solid phase, which are result of thermal decomposition of $FeSO_4 \cdot H_2O$ and $FeSO_4$. Thus, the process is controlled by the temperature, the regime of heating and the partial pressures of oxygen, water vapour and sulphur oxides.

Effect of temperature

The temperature ranges, where solid-phase synthesis of intermediate ferric sulphates occurs, the thermal stability and the desulphurisation depend on the temperature. The obtained results show that $FeOHSO_4$ is formed at lower temperatures 450–600 K and remains stable to 700 K. At temperatures higher than 700 K, $FeOHSO_4$ is transformed into $Fe_2O(SO_4)_2$ [18–20].

The $Fe_2O(SO_4)_2$ is the higher temperature modification with temperature range of formation between 680 and 810 K. The obtaining of iron oxysulphate is still a contentious issue due to the specific conditions in the reaction space, which are necessary to ensure, especially the content both of the oxygen and the water vapour. According to the phase diagram of the Fe–S–O system (Fig. 5) [18, 20] even at very low partial pressure of oxygen the oxidation of Fe^{2+} to Fe^{3+} is possible with obtaining metastable ferric sulphates. This synthesis can be performed in gaseous environments with different oxygen content—0% (pure Ar-inert environment), ~21% (dry air environment) and 100% (pure O_2 environment). The possible precursors are $FeSO_4 \cdot H_2O$ (dehydration and oxidation), $FeSO_4$ (oxidation and phase transition) and $FeOHSO_4$ (dehydration). The parameters, which can be taken into account, are the regime of heating (dynamic or isothermal), the rate of heating, the granulometry of sample and the quantity of sample in the crucible.

Thus, the structures of $Fe_2(SO_4)_3$ and $Fe_2O(SO_4)_2$ are similar, because one sulphate group of $Fe_2(SO_4)_3$ is replaced by an oxygen atom in $Fe_2O(SO_4)_2$. This is confirmed by experiments carried out with different methods (X-ray analysis, Mössbauer spectroscopy, Infrared spectroscopy—Figs. 1, Fig. 2, and 3). This fact explains the conflicting data, found in the references, on the formation and thermal decomposition of iron oxysulphate [1, 9, 13, 18–22].

The formation of oxygen bridge between two Fe^{3+} is a characteristic feature of the $Fe_2O(SO_4)_2$:

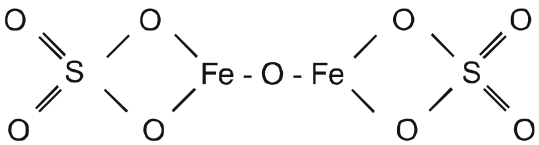

The nature of this relationship is area of special scientific interest. The oxygen bridge is formed at the dehydration of compounds, containing a hydroxyl ion, which is strongly associated with the other ions in the structure, such as hydroxyl-sulphates [2, 9, 18–21, 30–33], hydroxyl-apatites [34–46], hydrotalcites [47–56]. Some studies found that during the dehydration of these compounds an oxygen atom remains in their structure, which forms such type oxygen bridges. That means that for the accurate identification of $Fe_2O(SO_4)_2$ accurate methods, new techniques and a precise control of experimental conditions are necessary to use.

Influence of water vapour

The water vapour is an important factor in thermal decomposition of divalent iron sulphates. It is present in the reaction space as part of flowing gas or obtained by dehydration (structural or crystal water) of solid-phase samples. The water vapour pressure (P_{H_2O}), which is function of temperature, affects the process of decomposition by reaction (6). The partial pressure of a water vapour at constant other parameters (temperature and partial pressures of oxygen and sulphur oxides) shifts the equilibrium to more stable $FeOHSO_4$ and/or $Fe_2O(SO_4)_2$ (Fig. 5). With balanced values of the partial pressure of the water vapour at $T = 500$ K, both compounds in the system can be produced simultaneously. $FeOHSO_4$ is the thermally stable product at $P_{H_2O} > P_{H_2O_{(balanced)}}$; $Fe_2O(SO_4)_2$ at $P_{H_2O} < P_{H_2O_{(balanced)}}$. This means that at certain temperatures, as well as P_{O_2} and P_{SO_x}, the process may be controlled to obtain either monophase $FeOHSO_4$ or monophase $Fe_2O(SO_4)_2$.

The experiments do not confirm the oxidative action of oxygen from the OH^- at the dehydration of ferrous sulphate monohydrate in inert gas environment, which were published in [15]. This study with use of thermal, X-ray and spectroscopic methods found that after dehydration of $FeSO_4 \cdot H_2O$ in Ar flowing gas the anhydrous ferrous sulphate is obtained.

Influence of oxygen

The presence of oxygen in the reaction space in the processes of decomposition of $FeSO_4 \cdot H_2O$ and $FeSO_4$ always is linked oxidation of these divalent iron sulphates. The carried out experiments confirm that depending on the partial pressure of oxygen a different degree of oxidation is achieved. The experiments with use of pure oxygen as flowing gas show that the partial pressure of oxygen is not sufficient for the transformation of $FeSO_4 \cdot H_2O$ and $FeSO_4$ to $FeOHSO_4$ and/or $Fe_2O(SO_4)_2$. The high partial pressure

of oxygen is achieved only when pure oxygen is used as flowing gas, because the amount of oxygen is insufficient in flowing dry air. Nevertheless, the other parameters of the process (temperature and water vapour) must take into account. The high content of water vapour leads to obtain a mixture of $FeOHSO_4$ and $Fe_2O(SO_4)_2$. The ratio between these ferric sulphates depends on the temperature, the regime of heating and the heating rate.

The monophase compounds are obtained at the multiple constraints, as follows:

1. $FeSO_4$—inert gas environment (100% Ar, respectively $P_{O_2} \approx 0$); $P_{H_2O} \approx 0$; temperature range 520–600 K. The access of water vapour may be limited by use of dryers for reagent gases or fast remotion of water vapour from the reaction space.
2. $FeOHSO_4$—air or pure oxygen gas environment; overstoichiometric ratio between P_{H_2O} and P_{O_2} ($P_{H_2O} \gg P_{H_2O_{(balanced)}}$); temperature range 700–850 K. $FeSO_4 \cdot H_2O$ and $FeSO_4$ may be used as precursors.
3. $Fe_2O(SO_4)_2$—pure oxygen gas environment; $P_{O_2} \gg P_{H_2O}, P_{H_2O} \approx 0$; temperature range 810–815 K; isothermal mode of heating. $FeSO_4 \cdot H_2O$ and $FeSO_4$ may be used as precursors, but the use of $FeSO_4 \cdot H_2O$ creates difficulties, because of the presence of water vapour in the reaction space (when $T > 623$ K the $FeOHSO_4$ is obtained in the solid phase).
4. $Fe_2(SO_4)_3$—high partial pressure of sulphur oxides. This condition is achieved by use of gas environment saturated with sulphur oxides or by use of closed crucibles.

Conclusions

The parallel experiments prove that the thermal decomposition of $FeSO_4 \cdot H_2O$ and $FeSO_4$ in gas environments with various oxygen and water vapour contents leads to formation of both the $FeOHSO_4$ and $Fe_2O(SO_4)_2$ from the possible trivalent iron sulphates. The iron oxysulphate may be obtained in an inert gas environment, too. The partial pressure of oxygen depends on the degree of decomposition of ferrous sulphates to $Fe_2O(SO_4)_2$ in solid phase.

The presence of water vapour in the reaction space shifts the thermodynamic equilibrium of the Fe–S–O system to the formation of more stable $FeOHSO_4$. This process occurs if the partial pressure of the water vapour exceeds the equilibrium value at certain temperature. The $Fe_2O(SO_4)_2$ is more stable phase at partial pressures of water vapour below an equilibrium level. The end products of thermal decomposition of iron sulphates are a hematite and sulphur oxides. At the used experimental conditions (high partial pressure of oxygen, low partial pressure both of the water vapour and the sulphur oxides) the formation of $Fe_2(SO_4)_3$ as intermediate product of decomposition is not observed.

On the basis of comparative thermal investigation the main reactions, which describe the process of decomposition of $FeSO_4 \cdot H_2O$ and $FeSO_4$, are proposed. The path of reaction depends on the temperature regime, the regime of heating and the partial pressures of oxygen, the water vapour and the sulphur oxides. The obtained products give the possibility to consider the future of green technologies with recycling of iron and sulphur.

Acknowledgements Authors gratefully acknowledge the financial support of this study by the Bulgarian National Scientific Research Fund by contract DRNF02/10.

References

1. Zboril R, Mashlan M, Papaefthymiou V, Hadjipanayis G. Thermal decomposition of $Fe_2(SO_4)_3$: demonstration of Fe_2O_3 polymorphism. J Radioanal Nucl Chem. 2003;255(3):413–7.
2. Zboril R, Mashlan M, Petridis D. Polymorphous exhibitions of iron (III) oxide during isothermal oxidative decompositions of iron salts: a key role of the powder layer thickness. Chem Mater. 2002;14(3):969–82.
3. Solc Z, Trojan M, Brandova D, Kuchler M. A study of thermal preparation of iron (III) pigments by means of thermal analysis methods. J Therm Anal. 1988;3(2):463–9.
4. Šulcová P, Trojan M. Thermal synthesis and properties of the $(Bi_2O_3)_{1-x}(Ho_2O_3)_x$ pigments. J Therm Anal Calorim. 2006; 83(3):557–9.
5. Šulcová P, Trojan M. Thermal analysis of pigments based on Bi_2O_3. J Therm Anal Calorim. 2006;84(3):737–40.
6. Luxová J, Trojan M, Šulcová P. Application of mechanical activation for the synthesis of the pigment $ZnFe_2O_4$ with the spinel structure. Acta Metall Slovaca. 2005;11:437–49.
7. Mesíková Ž, Šulcová P, Trojan M. Yellow pigments based on Fe_2TiO_5 and TiO_2. J Therm Anal Calorim. 2006;83(3):561–3.
8. Mesíková Ž, Šulcová P, Trojan M. Preparation and practical application of spinel pigment $Co_{0.46}Zn_{0.55}(Ti_{0.064}Cr_{0.91})_2O_4$. J Therm Anal Calorim. 2006;84(3):733–6.
9. Zboril R, Mashlan M, Petridis D, Krausova D, Pikal P. The role of intermediates in the process of red ferric pigment manufacture from $FeSO_4.7H_2O$. Hyperfine Interact. 2002;139(1-4):437–45.
10. Kennedy T, Sturman BT. The oxidation of iron (II) sulphide. J Therm Anal. 1975;8:329–37.
11. Almeida C, Giannetti B. Comparative study of electrochemical and thermal oxidation of pyrite. J Solid State Electrochem. 2002;6:111–8.
12. Ferrow EA, Mannerstrand M, Berg B. Reaction kinetics and oxidation mechanisms of the conversion of pyrite to ferrous sulphate: a Mössbauer spectroscopy study. Hyperfine Interact. 2005;163:109–19.
13. Guilin Hu, Dam-Johansen Kim, Wede Stig, Peter Hansen Jens. Decomposition and oxidation of pyrite. Prog Energy Combust Sci. 2006;2:295–314.
14. Huiping Hu, Chen Qiyuan, Yin Zhoulan, Zhang Pingmin. Thermal behaviors of mechanically activated pyrites by thermogravimetry. Thermochim Acta. 2003;398:233–40.

15. Usher CR, JrCA Cleveland, Strongin DR, Schoonen MA. Origin of oxygen in sulphate during pyrite oxidation with water and dissolved oxygen: an in situ horizontal attenuated total reflectance infrared spectroscopy isotope study. Environ Sci Technol. 2004;38(21):5604–6.
16. Frost Ray L, Palmer Sara J, Kristóf J, Horváth E. Dynamic and controlled rate thermal analysis of halotrichite. J Therm Anal Calorim. 2010;99:501–7.
17. Navrotsky Al, Lázár Forray F, Drouet Ch. Jarosite stability on Mars. Icarus. 2005;176:250–3.
18. Pelovski Y, Petkova V, Nikolov S. Study of the mechanism of the thermochemical decomposition of ferrous sulphate monohydrate. Thermochim Acta. 1996;274:273–80.
19. Pelovski Y, Petkova V. Mechanism and kinetics of inorganic sulphates decomposition. J Therm Anal. 1997;49:1227–41.
20. Petkova V, Pelovski Y. Investigation on the thermal properties of $Fe_2O(SO_4)_2$: part I. J Therm Anal Calorim. 2001;64:1025–35.
21. Petkova V, Pelovski Y. Investigation on the Thermal Properties of $Fe_2O(SO_4)_2$: part II. J Therm Anal Calorim. 2001;64: 1037–44.
22. Petkova V, Pelovski Y. Comparative DSC study on thermal decomposition of iron sulphates. J Therm Anal Calorim. 2008; 93(3):847–52.
23. Krumm S. WINFIT 1.0.A computer program for X-ray diffraction line profile analysis. XIII Conference on Clay Mineralogy and Petrology. Acta Univ Carol Geol. 1994;38:253–61.
24. Kraus W, Nolze G. PowderCell—a program to visualize crystal structures, calculate the corresponding powder patterns and refine experimental curves. J Appl Cryst. 1996;29:301–3.
25. Powder Diffraction File Alphabetical Index, JCPDS, International Centre for Diffraction Data, Pennsylvania 19073–3273, sets 1–51:2001.
26. Nakamoto K. Infrared spectra of the inorganic and coordination compounds. 3rd ed. New York: Wiley; 1977. p. 153–4.
27. Masset P, Poinso JY, Poignet JC. TG/DTA/MS study of the thermal decomposition of $FeSO_4{\cdot}6H_2O$. J Therm Anal Calorim. 2006;83(2):457–62.
28. Broun ME, Dollimor D, Galwey AK. Reaction in the solid state. Amsterdam, Oxford, New York: Elsevier; 1980.
29. Scordari F. Crystal chemical implications on some alkali hydrated sulphates. Tsch Mineral Petrogr Mitt. 1981;28(3):207–22.
30. Scordari F, Ventruti G, Gualtieri Alessandro F. The structure of metahohmannite, $Fe_2^{3+}[O(SO_4)_2].4H_2O$, by in situ synchrotron. Am Mineral. 2004;89:365–70.
31. Ventruti G, Scordari F, Schingaro E, Gualtieri AF, Meneghini C. The order-disorder character of $FeOHSO_4$ obtained from the thermal decomposition of metahohmannite, $Fe_2^{3+}(H_2O)_4[O(SO_4)_2]$. Am Mineral. 2005;90(4):679–86.
32. Majzlan J, Navrotsky Al, Blainemccleskey R, ChN Alpers. Thermodynamic properties and crystal structure refinement of ferricopiapite, coquimbite, rhomboclase, and $Fe_2(SO_4)_3(H_2O)_5$. Eur J Mineral. 2006;18:175–86.
33. Majzlan J, Navrotsky Al, Schwertmann U. Thermodynamics of iron oxides: part III. Enthalpies of formation and stability of ferrihydrite ($\sim Fe(OH)_3$), schwertmannite ($\sim FeO(OH)_{3/4}(SO_4)_{1/8}$), and ε-Fe_2O_3. Geochim Cosmochim Acta. 2004;68(5): 1049–59.
34. Tõnsuaadu K, Gruselle M, Villain F, Thouvenot R, Peld M, Mikli V, Traksmaa R, Gredin P, Carrier X, Salles L. A new glance at ruthenium sorption mechanism on hydroxy, carbonate, and fluor apatites: analytical and structural studies. J Colloid Interface Sci. 2006;304(2):283–91.
35. Sherina Peroos, Zhimei Du, de Leeuw NH. A computer modelling study of the uptake, structure and distribution of carbonate defects in hydroxy-apatite. Biomaterials. 2006;27(9): 2150–61.
36. Tônsuaadu K, Peld M, Leskelä T, Mannonen R, Niinistö L, Veiderma M. A thermoanalytical study of synthetic carbonate-containing apatites. Thermochim Acta. 1995;256(1):55–65.
37. Wiria FE, Leong KF, Chua CK, Liu Y. Poly-ε-caprolactone/hydroxyapatite for tissue engineering scaffold fabrication via selective laser sintering. Acta Biomater. 2007;3(1):1–12.
38. Jokanović V, Jokanović B, Marković D, Živojinović V, Pašalić S, Izvonar D, Plavšić M. Kinetics and sintering mechanisms of hydro-thermally obtained hydroxyapatite. Mater Chem Phys. 2008;111(1):180–5.
39. Bianco A, Cacciotti I, Lombardi M, Montanaro L. Si-substituted hydroxyapatite nanopowders: synthesis, thermal stability and sinterability. Mater Res Bull. 2009;44(2):345–54.
40. He QJ, Huang ZL, Cheng XK, Yu J. Thermal stability of porous A-type carbonated hydroxyapatite spheres. Mater Lett. 2008;62(3): 539–42.
41. Lafon JP, Champion E, Bernache-Assollant D, Gibert R, Danna AM. Thermal decomposition of carbonated calcium phosphate apatites. J Therm Anal Calorim. 2003;72:1127–34.
42. Kannan S, Ventura JMG, Ferreira JMF. Synthesis and thermal stability of potassium substituted hydroxyapatites and hydroxyapatite/β-tricalciumphosphate mixtures. Ceram Int. 2007;33(8): 1489–94.
43. Stoyanov V. Rheological characteristics of cement pastes, determined by rotational viscometers. In: Proceedings of the X-th international conference on mechanics and technology of composite materials, vol 15–17, Sofia, Bulgaria, September; 2003. pp. 213–8.
44. Ivanov Ya., Stoyanov V, Kotsilkova R. Rheological estimation of methods for concrete design. In: Proceedings of the XIII-th international congress on rheology, vol 20–25, Cambridge, UK, August; 2000. pp. 205–7.
45. Ivanov Ya, Yanovsky Yu, Stoyanov V, Karnet Yu, On the influence of interface layers on the properties of polymer nanocomposites, In: Proceedings of the III-rd National Seminar on Nanotechnology, Sofia, Bulgaria, November 30—December 1, 2001, Nanoscience & Nanotechnology '02, Balabanova E and Dragieva I editors, Sofia: Heron Press; 2002. pp. 107–9.
46. Lajmi B, Hidouri M, Wattiaux A, Fournés L, Darriet J, Ben Amara M. Crystal structure, Mössbauer spectroscopy, and magnetic properties of a new potassium iron oxyphosphate $K_{11}Fe_{15}(PO_4)_{18}O$ related to the Langbeinite-like compounds. J Alloys Compd. 2003;361(1–2):77–83.
47. Hibino T, Yasumasa Y, Katsunori K, Atsumu T. Decarbonation behavior of Mg–Al–CO_3 hydrotalcite-like compounds during heat treatment. Clays Clay Miner. 1995;43(4):427–32.
48. Petrova N, Mizota T, Fujiwara K. Hydration heats of zeolites for evaluation as heat exchangers. J Therm Anal Calorim. 2001; 64:157.
49. Mizota T, Petrova N, Nakayama N. Entropy of zeolitic water. J Therm Anal Calorim. 2001;64:211–7.
50. Stanimirova Ts, Petrova N. DTA and TG study of minerals from the hydrotalcite–takovite isomorphic series: II. Influence of M^{2+}/M^{3+} cation ratio. Compt Rend Acad Bulg Sci. 1999;52(11-12): 59–62.
51. Stanimirova Ts, Piperov N, Petrova N, Kirov G. Thermal evolution of Mg–Al–CO_3 hydrotalcites. Clay Miner. 2004;39(2): 177–91.
52. Petrova N, Mizota T, Stanimirova Ts, Kirov G. Sorption of water vapor on a low-temperature hydrotalcite metaphase: calorimetric study. Microporous Mesoporous Mater. 2003;63(1-3): 139–45.
53. Stanimirova Ts, Vergilov I, Kirov G, Petrova N. Thermal decomposition products of hydrotalcite-like compounds: low-temperature metaphases. J Mater Sci. 1999;34(17):4153–61.

54. Holgado MJ, Labajos FM, Montero MJS, Rives V. Thermal decomposition of Mg/V hydrotalcites and catalytic performance of the products in oxidative dehydrogenation reactions. Mater Res Bull. 2003;38:1879–91.
55. Stoyanov V. A concept of the rheological behaviour of suspensions, In: Progress and trends in rheology, Emri I editor, In: Proceedings of the V-th European Rheology Conference, Slovenia, Portoroz; 1998. pp. 597–598.
56. Yörükoğulları E, Yilmaz G, Dikmen S. Thermal treatment of zeolitic tuff. J Therm Anal Calorim. 2010;100(3):925–8.